Enhancing the rheological properties and thermal stability of 1 oil-based drilling fluids by synergetic use of organo-montmorillonite and organo-sepiolite

Guanzheng Zhuang, Zepeng Zhang, Shanmao Peng, Jiahua Gao, Maguy Jaber

▶ **To cite this version:**

Guanzheng Zhuang, Zepeng Zhang, Shanmao Peng, Jiahua Gao, Maguy Jaber. Enhancing the rheological properties and thermal stability of 1 oil-based drilling fluids by synergetic use of organo-montmorillonite and organo-sepiolite. Applied Clay Science, 2018, 8220 (Septembre 2018), pp.505-512. 10.1016/j.clay.2018.05.018 . hal-01957994

HAL Id: hal-01957994

https://hal.sorbonne-universite.fr/hal-01957994

Submitted on 17 Dec 2018

HAL is a multi-disciplinary open access archive for the deposit and dissemination of scientific research documents, whether they are published or not. The documents may come from teaching and research institutions in France or abroad, or from public or private research centers.

L'archive ouverte pluridisciplinaire **HAL**, est destinée au dépôt et à la diffusion de documents scientifiques de niveau recherche, publiés ou non, émanant des établissements d'enseignement et de recherche français ou étrangers, des laboratoires publics ou privés.

Enhancing the rheological properties and thermal stability of oil-based drilling fluids by synergetic use of organo-montmorillonite and organo-sepiolite

Guanzheng Zhuang [a], Zepeng Zhang [a,*], Shanmao Peng [a], Jiahua Gao [a], Maguy Jaber [b,*]

[a] Beijing Key Laboratory of Materials Utilization of Nonmetallic Minerals and Solid Wastes, National Laboratory of Mineral Materials, School of Materials Science and Technology, China University of Geosciences, Xueyuan Road, Haidian District, Beijing 100083, PR China.

[b] Sorbonne Université, Laboratoire d'Archéologie Moléculaire et Structurale (LAMS), CNRS UMR 8220, case courrier 225, UPMC 4 Pl. Jussieu, 75005 PARIS CEDEX 05, France.

Corresponding Author:

Zepeng Zhang

Tel: +86-010-8232-1845

Email: unite508@163.com

Maguy Jaber

Tel: +33-(0)1-4427-6289

Email: maguy.jaber@upmc.fr

Abstract

This work focused on improving the rheological properties and thermal stability of oil-based drilling fluids by using the mixture of organo-montmorillonite (OMt) and organo-sepiolite (OSep) as the rheological additive. OMt and OSep were prepared in water. X-ray diffraction (XRD), scanning electron microscope and transmission electron microscope were applied to characterize the structure of organoclays (OC). The OC/oil gels were characterized using an appropriate XRD method. Dynamic rheological test was used to appraise the rheological behavior, viscosity, gel strength and thixotropy of OC/oil fluids aged at different temperatures. OMt firstly swelled in oil at low temperature, and then exfoliated above 150°C. OSep maintained its crystal structure all the time. The mixing of these two OC did not obviously influence their structures. However, the gel formation ability was promoted, resulting in improvement of rheological properties and thermal stability of oil-based drilling fluids. The nanolayers of OMt and nanofibers of OSep interweaved with each other, reinforcing the network structure and protected them form collapse at high temperatures. The mixture of OMt and OSep with mass proportion of 50% for each displayed the optimal rheological properties and thermal ability.

Keywords: Sepiolite, oil-based muds, rheological properties, organic modification, high temperature.

1. Introduction

Over the next 30 years, global energy is projected to rise almost 60%, a challenging trend that may be met only by revolutionary breakthroughs in energy science and technology (Esmaeili, 2011). Although the technologies of some new or renewable energies (such as new battery, wind energy, nuclear energy, etc.) are developing fast, oil and gas, as the traditional energy, are the main energy resource in the world. The demand of oil and gas is increasing due to the rapid development of the society. However, the petroleum industry is increasingly drilling more technically challenging and difficult wells. Drilling of deeper wells worldwide requires constants searching for adequate drilling fluids to overcome extreme conditions (Williams et al., 2011).

Drilling fluids are compared as “the bloods of drilling operations”. By drilling operations, oil and gas can be extracted from the earth. Drilling fluids serve several fundamental functions, such as (i) to remove the cuttings generated by the drill bit from the borehole, (ii) to control the downhole formation pressures, (iii) to overcome the fluid pressure of the formation, (iv) to avoid damage to the producing formation and (v) to cool and lubricate the drill bit, etc. (Chilingarian and Vorabutr, 1983; Caenn and Chillingar, 1996; Meng et al., 2012). Generally, drilling fluids can be divided into two types based on the continuous phase, i.e., water-based drilling fluids and oil-based drilling fluids. Water-based drilling fluids are limited by their abilities of dissolving salts, interfering with the flow of oil and gas through porous rocks, promoting the disintegration and dispersion of clay minerals, and effecting the corrosion of iron

(Caenn et al., 2011). Oil-based drilling fluids, owing to their excellent lubricity, high rate of penetration, shale inhibition, wellbore stability, high lubricity, high thermal stability (Caenn and Chillingar, 1996; Khodja et al., 2010), are advised to be used to drill difficult wells. In spite of the advantages of oil-based drilling fluids, drilling practice always demand drilling fluids with greater rheological properties and better thermal stability.

Organoclays (OC) are used in oil-based drilling fluids to control the rheological behavior. They perform specific functions in a base oil and are varied in amount to furnish the properties required for satisfying the conditions of use. Organo-montmorillonite (OMt) is mostly used in oil-based drilling fluids (Caenn et al., 2011; Dino and Thompson, 2013; Zhuang et al., 2016, 2017b). Hermoso et al. (2014) reported that the viscous flow behavior of oil-based drilling fluids is deeply influenced by OMt nature and concentration. (Schmidt, 1987) proposed that OC did not viscosify the oils but built the structure through interactions with the aqueous face (water phase is usually included in oil-based drilling fluids). But later work (Burgentzle et al., 2004) demonstrated that OMt can viscosify organic solvents without water. Previous work (Zhuang et al., 2017b, d) reported the exfoliation of OMt in oil aged at high temperatures. Exfoliated OMt produced many nanolayers to build a “house of cards” structure, resulting in the improvement of gel formation and rheological properties. By comparing studies on different modifiers, surfactants containing two long alkyl chains was proved to be easier to result in exfoliation of OMt in oil and excellent rheological properties. However, distinct decline of the rheological properties occurred when best

89 fluids aged above 180°C, because of two potential ways, i.e., thermal decomposition
90 and desorption of organic surfactants.

91 Recently, the OC from palygorskite-sepiolite family were reported to be used in oil-
92 based drilling fluids (Dino and Thompson, 2002; Zhuang et al., 2017a, c, d, 2018b;
93 Weng et al., 2018). They exhibited excellent rheological properties in oil by forming a
94 “haystack” structure. These clay minerals are natural nanofibrous materials. For
95 sepiolite (Sep), its fiber sizes generally range from 0.2 μm to 2 μm in length, 100 nm to
96 300 nm in width and 50 nm to 100 nm in thickness (Alvarez, 1984; Álvarez et al., 2011).
97 Accordingly, Sep shows preeminent rheological properties in polar solvents. By organic
98 modification, organo-sepiolite (OSep) displays the lipophilicity and can perform
99 excellent rheological properties in oil (Zhuang et al., 2018a).

100 Some recent literature reported about the joint use of Mt and fibrous clay minerals
101 (Neaman and Singer, 2000; Chemeda et al., 2014; Al-Malki et al., 2016) to enhance the
102 rheological properties of clay minerals in solvents. Al-Malki et al. (2016) found that
103 bentonite-based drilling mud with Sep nanoparticles showed a great stability in plastic
104 viscosity and yield point over a wide range of temperature and pressure, especially at
105 high temperatures and pressures. The previous work enlightened that synergistic use of
106 OMt and OSep may also promote the rheological properties and thermal stability of oil-
107 based drilling fluids. This is a promising way to sustain oil-based drilling fluids work
108 in difficult wells.

109 Aiming to improve the rheological properties and thermal stability of oil-based
110 drilling fluids, OMt and OSep was synergistically used in oil-based fluids aged at

different temperatures and their structures and rheological properties were characterized.

2. Materials and Methods

2.1 Materials

Na^+-treated Mt was obtained from Kazuo, Liaoning, China, with the purity of ca. 84% and cation exchange capacity (CEC) of 120 cmol/kg. Sep was obtained from Spain, with the CEC of 35 cmol/kg. The purity of clay minerals was defined X-Ray diffraction method according to the Chinese standard SY/T 5163-2010. Details of this method were reported in previous literature (Zhuang et al., 2018a). Some quartz (12%), calcite (4%) and albite (2%) were included in the Mt sample (see Fig. 1 (A)). XRD pattern of Sep (Fig. 1 (B)) matches well with the JCPDS card of Sep and no other reflections are observed, indicating the high purity of Sep. The chemical composition of Mt and Sep were characterized by X-ray fluorescence (XRF) analysis and the results are listed in Table 1. Both of these two clay minerals were milled and sieved with a 200-mesh sieve before use. Benzyl dimethyl octadecyl ammonium chloride (C18, purity of 97%) and dimethyl dioctadecyl ammonium chloride (DC18, purity of 98%) were bought from Anhui Super Chemical Technology Co., Ltd, China. The white oil (No. 5) was bought from China National Petroleum Corporation.

2.2 Preparation of OC

OMt was prepared in aqueous solution as the following steps: 100 g of Mt was

added into 1 L deionized water, stirring for 0.5 h; then DC18 (1.0 CEC of Mt) was added into the previous dispersion, stirring for 1 h; at last, by centrifugation, drying at 60°C for 24 h, milling and sieving with a 200-mesh sieve. OSep was prepared as the following steps: C18 (35% of the mass of Sep) was firstly dissolved into 500 mL distilled water (keep at 60°C in the whole process), 100 g of Sep was added into the previous solution, stirred for 1 h and thickened slurry was obtained; at last, after drying at 60°C for 24 h, milling and sieving with a 200-mesh sieve, OSep was prepared.

2.3 Preparation of Sep/oil fluids

12 g of OC was added into 400 mL white oil (concentration of 30 kg/m^3) and blended at 10000 rpm for 20 min. A drilling fluid should be aged at different temperatures to model the real drilling operation. According to the standards of API SPEC 13A and API RP 13B-2, the resulting fluid was placed in a rotary oven heated to 66°C, 150°C, 180°C and 200°C where it was aged for 16 h. The mixtures of OC in oil-based drilling fluids are listed in Table 2. The corresponding fluid is named as OC/oil-temperature. For example, the oil-based fluid of $OMt_{0.5}$-$OSep_{0.5}$ and oil aged at 150°C is named as $OMt_{0.5}$-$OSep_{0.5}$/oil-150.

2.4 Characterization

The X-ray diffraction (XRD) analysis was conducted on a Bruker D8 Advance X-ray powder diffractometer operating at Cu Kα radiation, 40 kV, 40 mA and a scan speed of 0.05 s per step (step size: 0.02°). The XRD patterns were collected from 3° to 70°. Particularly, the XRD test for OC/oil gels is described in the section 3.1. Scanning

electron microscope (SEM) images were obtained with a HITACHI SU8000 type SEM and the operating voltage was 10 kV. The transmission electron microscope (TEM) analysis was conducted on a JEM 1200EX TEM equipment and operated at the voltage of 200 kV. Gel volume results were obtained by adding 100 mL aged fluid into a graduated cylinder with a stopper and standing for 24 h. The dynamic rheological behavior of oil-based fluids was tested by a Thermo Scientific HAAKE Roto Visco 1 rotational viscometer at 20°C. The tested program was: the shear rate linearly increased from 0 s^{-1} to 100 s^{-1} in 5 min (up step), and then linearly decreased from 100 s^{-1} to 0 s^{-1} in 5 min (down step).

3. Results and discussion

3.1 XRD analysis

The XRD patterns of Mt and OMt were presented in Fig. 1 (A). There were some impurities, i.e., quartz and calcite in the Mt sample. The basal reflection of Mt occurred at $2\theta = 7.05°$, with the basal spacing of 1.25 nm. Modified with DC18, a group of reflections emerged at 2.40°, 4.82° and 7.34°, which were attributed to the reflections of (001), (002) and (003) crystalline planes. The basal spacing of OMt increased to 3.68 nm, indicating the successful intercalation of DC18 into the interlayer space. In Fig. 1 (B), the XRD pattern of OSep is nearly the same with that of Sep. This phenomenon demonstrated that the organic modification could not influence the crystal structure of Sep, similar with the modification of palygorskite (Zhuang et al., 2017a, c). This is because that the TOT (T refers [SiO_4] tetrahedron and O refers to [$Al(Mg)O_6$]

177 octahedron) layers were linked by covalent bonds. Based on the TGA results (see Fig.
178 S1, in supplementary materials), there were 40.8% and 23.4% of organic surfactants
179 included in OMt and OSep, respectively.

180 The OC/oil gels were also characterized by XRD using an appropriate method (see
181 Fig. 2 (A)). Firstly, the OC/oil fluid was dripped on oil-absorbing papers. After 24 h of
182 natural absorption, extra oil was removed and the OC/oil gel was obtained. OC/oil gels
183 were marked following the template of “OC/oil-temperature”. Finally, the OC/oil gels
184 can be tested using the X-ray diffractometer similar with powder samples. The XRD
185 patterns of sample holder and sample holder with oil are shown in Fig. 2 (B). The
186 sample holder exhibited a small reflection with low intensity. However, a wider
187 reflection occurred in the XRD pattern of sample holder + oil, with higher intensity.
188 These two reflections are typical amorphous ones, in agreement with the previous
189 literature (Ribotta et al., 2004; Bates et al., 2006; Ford et al., 2010; Rowe and Brewer,
190 2017). Thus, this reflection between 8 to 30° and centering at ca. 17° is assigned to the
191 amorphous reflection of oil.

192 The XRD patterns of OC/oil gels aged at different temperatures are presented in Fig.
193 3. A wide reflection in the range of 2θ = 8-30° emerged in the XRD patterns of OC/oil
194 gels, centering at 17 to 18°. They are attributed to the oil as proved in Fig. 2 (B). These
195 wide reflections demonstrated that oil molecules were packaged in the network
196 structures of OC. The intensity of these reflections can be used to evaluate the oil
197 contents in the gels. Compared with OMt, the XRD patterns of OMt/oil-66 and $OMt_{0.8}$-
198 $OSep_{0.2}$/oil-66 showed that the basal spacing of OMt in these two gels increased to 5.04

nm: indeed, oil molecules are probably in the interlayer space due to the lipophilicity. In the XRD pattern of $OMt_{0.5}$-$OSep_{0.5}$/oil-66, both intensities of reflections attributed to OMt and OSep dramatically reduced, indicating disordered arrangements parallel to the c-axis of OMt and the b-axis of OSep. When the mass content of OSep increased to 80%, the basal reflection of OMt disappeared in the XRD pattern of $OMt_{0.2}$-$OSep_{0.8}$/oil-66. Considering the changes in the XRD patterns of $OMt_{0.5}$-$OSep_{0.5}$/oil-66 and $OMt_{0.2}$-$OSep_{0.8}$/oil-66, the mixing of OMt and OSep facilitated the exfoliation of OMt. The XRD pattern of OSep/oil-66 is similar with that of OSep powder, in spite of the wide reflection from 8° to 30°.

With the temperature rising, the wide reflection of oil showed high intensity, indicating more oil molecules contained in the gel structures. This fact proved that high temperatures promoted the formation of a stronger network structure with large interspace. OSep/oil gels maintained the reflections of Sep at different temperatures. However, the basal reflections of OMt/oil gels aged above 150°C disappeared, probably suggesting the exfoliation of OMt. But the (100) reflection, which emerged at 2θ = 19.7°, was kept in the XRD patterns of OMt/oil gels. This phenomenon implied that the individual TOT structures were kept and changes just happened to the arrangement paralleling to the c-axis. The basal reflection of OMt was not observed in the mixture of OMt and OSep aged at high temperatures, indicating the exfoliation of OMt. With the increase of OSep, OC/oil gels exhibited higher intensity of the (110) reflection, because of the more proportion of OSep. Significantly, the XRD patterns of these OC/oil aged from 150°C to 200°C showed the similar reflections, indicating that they

kept the structures in this temperature range.

3.2 SEM and TEM

The SEM and TEM images are presented in Fig. 4. OMt is associated with a large number of silicate layers. To some extent, these layers are soft so that they may be curved. Based on the TEM image of OMt, the lamellae contain at least 10 layers. The distance between two adjacent layers was measured as 3.56 nm. This value is a little smaller than the basal spacing derived from the XRD result. This is because the high voltage of TEM test (200 kV) would destroy the interlayer surfactants and/or dehydration of the interlayer space (Kogure, 2013). Hence, the basal spacing calculated from the TEM depended on the voltage, test time, thermal stability of organic compounds and the thickness of samples. The exfoliation of OMt was defined as no further interaction occurs between the two delaminated units (isolated layers or stacking of few layers) which become independently mobile in the liquid phase (Bergaya et al., 2012), so that the no long-range order was apparent along the c-axis. The exfoliated OMt layers would form a “house of cards” structure by surface to edge and edge to edge arrangements.

The SEM and TEM images of OSep showed the disordered aggregation of OSep fibers. The length of fibers ranged from hundreds of nanometers to ca. 1 μm. Indeed, the OSep existed in the forms of individual fibers (rods), laths and bundles (García-Romero and Suárez, 2013). The crystal laths and bundles, which consist of nanofibers, are very hard to be disaggregated, due to the electronic attraction, Van der Waals forces

and hydrogen bonding interaction (Haden and Schwint, 1967; Xu et al., 2014). The aggregation of different forms of OSep built a “haystack” structure (Haden, 1963).

The SEM or TEM images of OC/oil gels can’t be obtained, because of the high amount of oil present in the gels. Indeed, it is difficult to remove the oil because of its high boiling point and non-volatile ability.

3.3 Gel volume

The gel volume results (see Fig. 5) can directly show the gel formation ability and compatibility between oil and OC. At the initial time (t = 0 s), all the gel volumes of OC/oil fluids were set as 100.0 mL. When the time went to 90 min, the gel volumes of OMt, $OMt_{0.8}$-$OSep_{0.2}$, $OMt_{0.5}$-$OSep_{0.5}$, $OMt_{0.2}$-$OSep_{0.8}$ and OSep in oil were 21.8 mL, 97.2 mL, 98.0 mL, 100.0 mL and 100.0 mL, respectively. After standing four 24 h, the gel volumes became 15.7 mL for OMt, 67.1 mL for $OMt_{0.8}$-$OSep_{0.2}$, 89.5 mL for $OMt_{0.5}$-$OSep_{0.5}$, 100.0 mL for $OMt_{0.2}$-$OSep_{0.8}$ and 100.0 mL for OSep. OMt showed the least gel volume in oil while OSep presented the gel volume of 100.0 mL. At room temperature, OMt can only absorb a part of oil molecules, resulting in the expanding of interlayer space. The swelling OMt particles dispersed and stacked in oil, without prominent contributions to promoting the network structure and gel formation. However, TEM images testified that OSep is in the form of fibers, laths and bundles, which are in nanoscale. These fibers laths and bundles could be easier to form “haystack” structures, leading to the high and stable gel volumes. The gel volumes of OMt/OSep mixture in oil increased with the increase of OSep proportion. This phenomenon

suggested that the addition of OSep contributed to the gel formation of OMt in oil.

3.4 Rheological properties

The dynamic rheological curves of OC/oil fluids are presented in Fig. 6. These curves display the rheological behavior and thermal stability of corresponding OC/oil fluids. Aged at 66°C, OMt/oil fluid showed the highest shear stress, indicating that OMt/oil fluid displayed the best viscosity. OMt/oil and OSep/oil fluids aged at 66°C showed the different curves of up step and down step. However, in the rheological curves of the mixture of OMt and OSep fluids, the down step curves nearly followed the up step curves. This fact demonstrated that the network structures of OMt and OSep in oil obviously changed while no distinct structural changes happened in the mixture fluids. The single OC built their own network structures in oil. But the new network structure didn't form well in the mixed oil fluids aged at 66°C. In addition, the rheological curves of fluids aged at 66°C followed the Bingham plastic model at 10-100 s^{-1}, except for OSep/oil aged at 66°C.

When the temperature increased to above 150°C, the rheological curves became very different. Firstly, the shear stresses of fluids aged above 150°C is much larger than those of fluids aged at 66°C, demonstrating the promotion of network structures and viscosity by high temperatures. Furthermore, in the up step, a rapid climb was observed before 20 s^{-1}, and then a dramatical decline occurred. Consequently, there was a critical point which showed the highest shear stress. This critical point suggested that a large shear stress must be applied to break the connected aggregates

of OC and to disperse and orient stacked nanoplatelets or nanofibers (maybe nano laths and bundles) in the flow direction (Zhuang et al., 2017b). In the down step, the curves were nearly lines (in spite of the derivation at 0-20 s^{-1}), in agreement with the Bingham plastic model. No critical points were seen in the down step because the network had been sheared at high shear rate and the network structures were destroyed.

These critical points can indicate the gel strengths of network structures. The shear stress results corresponding to these critical points are listed in Table 3. Aged at 66°C, OSep/oil fluid showed a little different rheological curve from other fluids, due to the changes at 0-40 s^{-1} in up step. It was a critical range, instead of a point, because the network structure was not enough strong. The critical shear stresses of OMt/oil and OSep/oil fluids firstly increased and then decreased, indicating that the increase of aging temperature firstly improved the formation of network structure and higher temperature would be harmful for the network structure, due to the thermal degradation and/or desorption of organic surfactants. The critical shear stress of $OMt_{0.8}$-$OSep_{0.2}$/oil fluid gradually decreased with the temperature rising. However, $OMt_{0.5}$-$OSep_{0.5}$/oil and $OMt_{0.2}$-$OSep_{0.8}$/oil fluids showed basically stable critical shear stresses from 150°C to 180°C, and little higher ones at 200°C. This phenomenon demonstrated the better stability of the mixture of OMt and OSep than single OC in oil-based drilling fluids.

The shear stresses of samples at 100 s^{-1} were applied to evaluate the viscosities (η) of different fluids (Table 4). As $\eta = \tau/\gamma$ and γ was constant (τ refers to shear stress and

309 γ refers to shear rate), i.e., 100 s^{-1}, τ can be used to indicate the changes of η. Aged at
310 66°C, the τ values of samples were very low, because the OC were not exfoliated
311 completely or dispersed well. With the temperature rising, the τ values dramatically
312 increased due to the fine formation of network structures which was promoted by high
313 temperatures. For example, the $\tau_{66\text{-}150}$ values of OMt/oil, $OMt_{0.8}$-$OSep_{0.2}$/oil, $OMt_{0.5}$-
314 $OSep_{0.5}$/oil, $OMt_{0.2}$-$OSep_{0.8}$/oil and OSep/oil were 108%, 378%, 687%, 696% and
315 694%. Compared with the τ values at 180°C, OMt/oil, $OMt_{0.8}$-$OSep_{0.2}$/oil and OSep/oil
316 at 200°C decreased by 49%, 26% and 18%. However, the τ values of $OMt_{0.5}$-$OSep_{0.5}$
317 and $OMt_{0.2}$-$OSep_{0.8}$ at 200°C increased by 46% and 18%. These results also supported
318 that the mixture of OMt and OSep benefited the viscosity and thermal stability of oil-
319 base drilling fluids.

320 Thixotropy represents a reversible isothermal transformation of a colloidal sol to
321 a gel. It is caused by the clay mineral units slowly arranging themselves in positions of
322 minimum free energy. In drilling practice, low resistance (low viscosity) is expected for
323 the bit to ensure high drilling rate, while high viscosity is expected for carrying cuttings.
324 Excellent thixotropy of an oil-based drilling fluid is necessary. The areas of thixotropic
325 loops (abbreviated as A, see in Table 5) in Fig. 6 are applied to evaluate the thixotropy
326 of OSep/oil fluids.

327 Aged at 66°C, the A value of OMt/oil fluid was 22.5 $Pa \cdot s^{-1}$ and that of OSep/oil
328 fluid was 39.38 $Pa \cdot s^{-1}$. The A values of $OMt_{0.8}$-$OSep_{0.2}$/oil, $OMt_{0.5}$-$OSep_{0.5}$/oil and
329 $OMt_{0.2}$-$OSep_{0.8}$/oil fluids ranged from 2.39 to 4.82 $Pa \cdot s^{-1}$, indicating nearly no
330 thixotropy of these samples. High temperatures promoted the gel formation. The A

values of samples increased until aged at 180°C, except for those of $OMt_{0.5}$-$OSep_{0.5}$/oil and $OMt_{0.2}$-$OSep_{0.8}$/oil. The decrease rates of OMt/oil, $OMt_{0.8}$-$OSep_{0.2}$/oil and OSep/oil from 180°C to 200°C ($A_{180\text{-}200}$) were 71%, 49% and 24%. OMt/oil declined more than OSep/oil. $OMt_{0.5}$-$OSep_{0.5}$/oil and $OMt_{0.2}$-$OSep_{0.8}$/oil exhibited continuous and slow augment of the A values until to 200°C, so that these two samples can be basically regarded as stable samples. The A values of $OMt_{0.5}$-$OSep_{0.5}$/oil and $OMt_{0.2}$-$OSep_{0.8}$/oil at 150-200°C were much more than those of a single OC, demonstrating that the mixture of OMt and OSep contributed to improving the thixotropy of oil-based fluids.

Considering all the discussions of rheological properties, the mixture of OMt and OSep, with the mass proportion of 50% for each, can effectively improve the viscosity, gel strength, thixotropy and thermal stability of the oil-based fluids.

3.5 Network structure

The rheological test proved that the $OMt_{0.5}$-$OSep_{0.5}$ performed greater rheological properties and better thermal stability in oil than each single OC did. This enhancement was resulted by the mixed network structure (see Fig. 7). When mixing OMt and OSep in oil, they firstly disperse following their own nature. At low temperature, oil molecules were adsorbed into the interlayer space of OMt, resulting in swelling. OMt was mostly in the form of swelled particles, perhaps with a little exfoliated nanolayers. OSep fibers, laths and crystal bundles dispersed in oil. Although the mass proportions of these two OC were identical, the number of OMt particles was much less than the

number of OSep fibers, laths and bundles. Due to the difference of these numbers, OMt and OSep had no strong contact with each other. But the mixing of these two OC still improved their gel formation in oil (see Fig. 5).

As the XRD results demonstrated that OMt exfoliated in oil above 150°C, one OMt particle might divided into dozens or hundreds of nanolayers. Consequently, the number of OMt layers dramatically increased. Influenced by the thermal motion, these nanolayers mixed and contact with the nanofibers, laths and bundles. Significantly, the "house of cards" structure of OMt and the "haystack" structure were not independent. These two different shapes of silicate units (layered OMt and fibrous OSep) interweaved with each other, leading to a stronger network structure. Previous work testified that organic surfactants would decomposed or/and dissolved into oil at high temperature, resulting the shrink of OMt (Zhuang et al. 2017b). In this mixed network structure, exfoliated OMt layers were supported by OSep fibers, and the OSep fibers were also sustained by the nanolayers.

4. Conclusion

In summary, synergetic use of OMt and OSep can improve the rheological properties and thermal stability of oil-based drilling fluids. OMt firstly swelled in oil by adsorbing oil molecules while OSep showed stable dispersion due to its nanoscale fibers, laths and bundles. At high temperature, thermal motion promoted the exfoliation of OMt into nanolayers. The interweave of nanofibers (laths and bundles) of nanolayers enhanced the network structure, resulting in improvement of rheological properties.

The mutual support between OMt nanolayers and OSep nanofibers protected this network structure form crush at high temperatures.

Acknowledgement

This work is financially supported by the Fundamental Research Funds for Central Universities (China, grant No. 2-9-2016-043) and the support provided by China Scholarship Council (CSC) during a visit of Guanzheng Zhuang (No. 201706400010) to Sorbonne Université is acknowledged.

References

Al-Malki, N., Pourafshary, P., Al-Hadrami, H., Abdo, J., 2016. Controlling bentonite-based drilling mud properties using sepiolite nanoparticles. Petrol. Explor. Dev. 43, 717-723.

Alvarez, A., 1984. Sepiolite: properties and uses, in: Tolsa (Ed.), Developments in Sedimentology, pp. 253-287.

Álvarez, A., Santarén, J., Esteban-Cubillo, A., Aparicio, P., 2011. Current Industrial Applications of Palygorskite and Sepiolite, in: Singer, A., Galan, E. (Eds.), Developments in Clay Science. Elsevier, Amsterdam, pp. 281-298.

Bates, S., Zografi, G., Engers, D., Morris, K., Crowley, K., & Newman, A. (2006). Analysis of amorphous and nanocrystalline solids from their X-ray diffraction patterns. Pharm. res., 23(10), 2333-2349.

Bergaya, F., Jaber, M., Lambert, J.F., Chapter 3 Clays and Clay Minerals as Layered

Nanofillers for (Bio)Polymers. In: Environmental Silicate Nano-biocomposites, Avérous, L. and Pollet, E (Eds) Springer London. 2012, 41-75

Burgentzle, D., Duchet, J., Gerard, J.F., Jupin, A., Fillon, B., 2004. Solvent-based nanocomposite coatings I. Dispersion of organophilic montmorillonite in organic solvents. J. Colloid. Interf. Sci., 278, 26-39.

Caenn, R., Chillingar, G.V., 1996. Drilling fluids: State of the art. J. Petrol. Sci. Eng., 14, 221-230.

Caenn, R., Darley, H.C., Gray, G.R., 2011. Composition and properties of drilling and completion fluids. Gulf professional publishing, Houston.

Chemeda, Y.C., Christidis, G.E., Khan, N.M.T., Koutsopoulou, E., Hatzistamou, V., Kelessidis, V.C., 2014. Rheological properties of palygorskite-bentonite and sepiolite-bentonite mixed clay suspensions. Appl. Clay Sci., 90, 165-174.

Chilingarian, G.V., Vorabutr, P., 1983. Drilling and drilling fluids. Elsevier Scientific Pub. Co. distributors for the U.S. and Canada, Elsevier North-Holland.

Dino, D., Thompson, J., 2002. Organophilic clay additives and oil well drilling fluids with less temperature dependent rheological properties containing said additives. US 6462096 B1.

Dino, D., Thompson, J., 2013. Organophilic clay additives and oil well drilling fluids with less temperature dependent rheological properties, US8389447 B2.

Esmaeili, A., 2011. Applications of Nanotechnology in Oil and Gas Industry, AIP conference proceedings, AIP 1414(1): 133-136.

Ford, E. N. J., Mendon, S. K., Thames, S. F., Ph., D., Rawlins, J. W., & Ph., D. (2010).

X-ray diffraction of cotton treated with neutralized vegetable oil-based macromolecular crosslinkers. J. Eng. Fiber Fabr., 5(1), 10-20.

García-Romero, E., Suárez, M., 2013. Sepiolite–palygorskite: Textural study and genetic considerations. Appl. Clay Sci., 86, 129-144.

Haden, W., 1963. Attapulgite: properties and uses. Clays Clay Miner 10, 284-290.

Haden, W.L., Schwint, I.A., 1967. Attapulglte: Its properties and applications. Ind. Eng. Chem., 59, 58-69.

Hermoso, J., Martinez-Boza, F., Gallegos, C., 2014. Influence of viscosity modifier nature and concentration on the viscous flow behaviour of oil-based drilling fluids at high pressure. Appl. Clay Sci., 87, 14-21.

Khodja, M., Canselier, J.P., Bergaya, F., Fourar, K., Khodja, M., Cohaut, N., Benmounah, A., 2010. Shale problems and water-based drilling fluid optimisation in the Hassi Messaoud Algerian oil field. Appl. Clay Sci., 49, 383-393.

Kogure, T., 2013. Chapter 2.9 - Electron Microscopy, in: Bergaya, F., Lagaly, G. (Eds.), Developments in Clay Science. Elsevier, Netherlands, pp. 275-317.

Meng, X., Zhang, Y., Zhou, F., Chu, P.K., 2012. Effects of carbon ash on rheological properties of water-based drilling fluids. J. Petrol. Sci. Eng., 100, 1-8.

Neaman, A., Singer, A., 2000. Rheology of mixed palygorskite-montmorillonite suspensions. Clay Clay Miner. 48, 713-715.

Ribotta, P. D., Cuffini, S., León, A. E., & Añón, M. C. (2004). The staling of bread: an x-ray diffraction study. Eur. Food Res. Technol., 218(3), 219-223.

Rowe, M. C., Brewer, B. J. (2017). AMORPH: A statistical program for characterizing

441 amorphous materials by X-ray diffraction. arXiv:1709.04556.
442 Schmidt, D.D., Roos, A. J., & Cline, J. T, 1987. Interaction of water with organophilic
443 clay in base oils to build viscosity. Society of Petroleum Engineers, 311-326.
444 Weng, J., Gong, Z., Liao, L., Lv, G., Tan, J., 2018. Comparison of organo-sepiolite
445 modified by different surfactants and their rheological behavior in oil-based
446 drilling fluids. Appl. Clay Sci., in press, DOI: 10.1016/j.clay.2017.12.031.
447 Williams, R.H., Khatri, D.K., Vaughan, M.L., Landry, G., Janner, L., Mutize, B.,
448 Herrera, M., 2011. Particle size distribution-engineered cementing approach
449 reduces need for polymeric extenders in haynesville shale horizontal reach wells,
450 SPE Annual Technical Conference and Exhibition. Society of Petroleum
451 Engineers.
452 Xu, J., Wang, W., Wang, A., 2014. Dispersion of palygorskite in ethanol–water mixtures
453 via high-pressure homogenization: Microstructure and colloidal properties.
454 Powder Technol., 261, 98-104.
455 Zhuang, G., Zhang, Z., Sun, J., Liao, L., 2016. The structure and rheology of organo-
456 montmorillonite in oil-based system aged under different temperatures. Appl. Clay
457 Sci., 124, 21-30.
458 Zhuang, G., Wu, H., Zhang, H., Zhang, Z., Zhang, X., Liao, L., 2017a. Rheological
459 properties of organo-palygorskite in oil-based drilling fluids aged at different
460 temperatures. Appl. Clay Sci., 137, 50-58.
461 Zhuang, G., Zhang, H., Wu, H., Zhang, Z., Liao, L., 2017b. Influence of the surfactants'
462 nature on the structure and rheology of organo-montmorillonite in oil-based

drilling fluids. Appl. Clay Sci., 135, 244-252.

Zhuang, G., Zhang, Z., Gao, J., Zhang, X., Liao, L., 2017c. Influences of surfactants on the structures and properties of organo-palygorskite in oil-based drilling fluids. Micropor. Mesopor. Mat., 244, 37-46.

Zhuang, G., Zhang, Z., Jaber, M., Gao, J., Peng, S., 2017d. Comparative study on the structures and properties of organo-montmorillonite and organo-palygorskite in oil-based drilling fluids. J. Ind. Eng. Chem., 56, 246-257.

Zhuang, G., Gao, J., Chen, H., Zhang, Z., 2018a. A new one-step method for physical purification and organic modification of sepiolite. Appl. Clay Sci., 153, 1-8.

Zhuang, G., Zhang, Z., Yang, H., Tan, J., 2018b. Structures and rheological properties of organo-sepiolite in oil-based drilling fluids. Appl. Clay Sci., 154, 43-51.

Figures

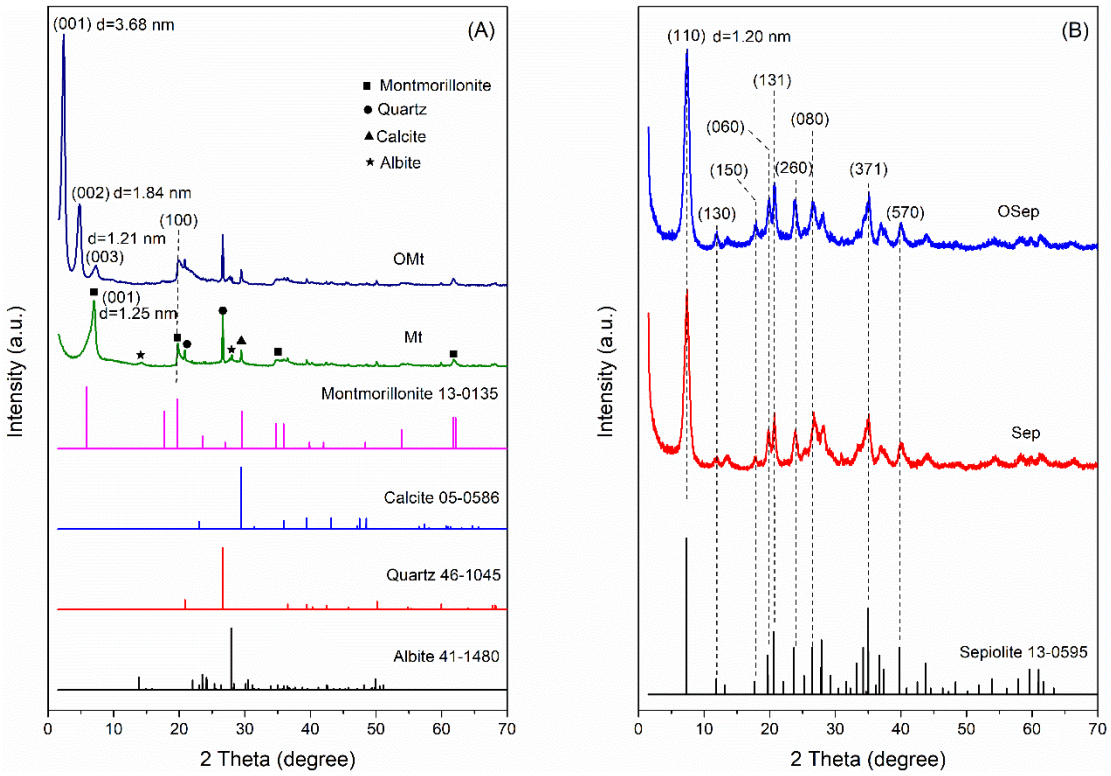

Fig. 1 XRD patterns of (A) Mt, OMt, (B) Sep and OSep.

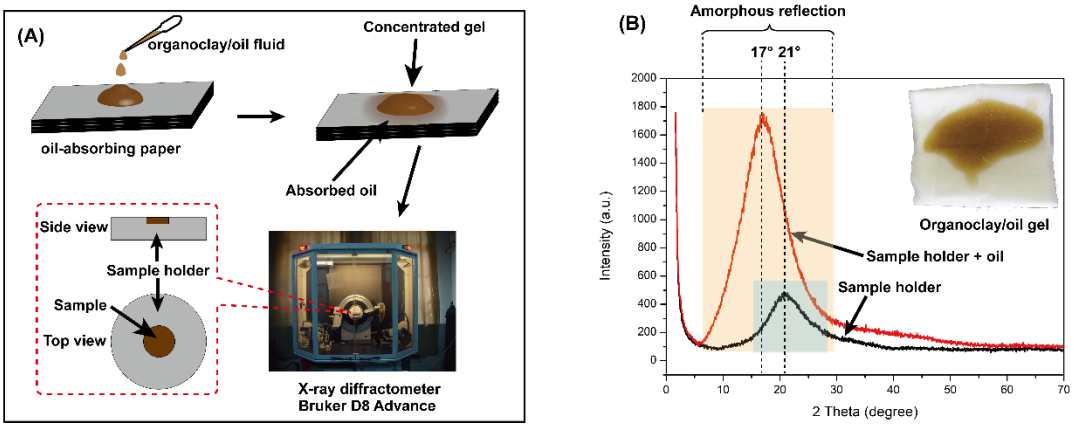

Fig. 2 (A) Interpretive diagram of XRD test for OC/oil gel sample and (B) XRD patterns of the sample holder and sample holder with oil.

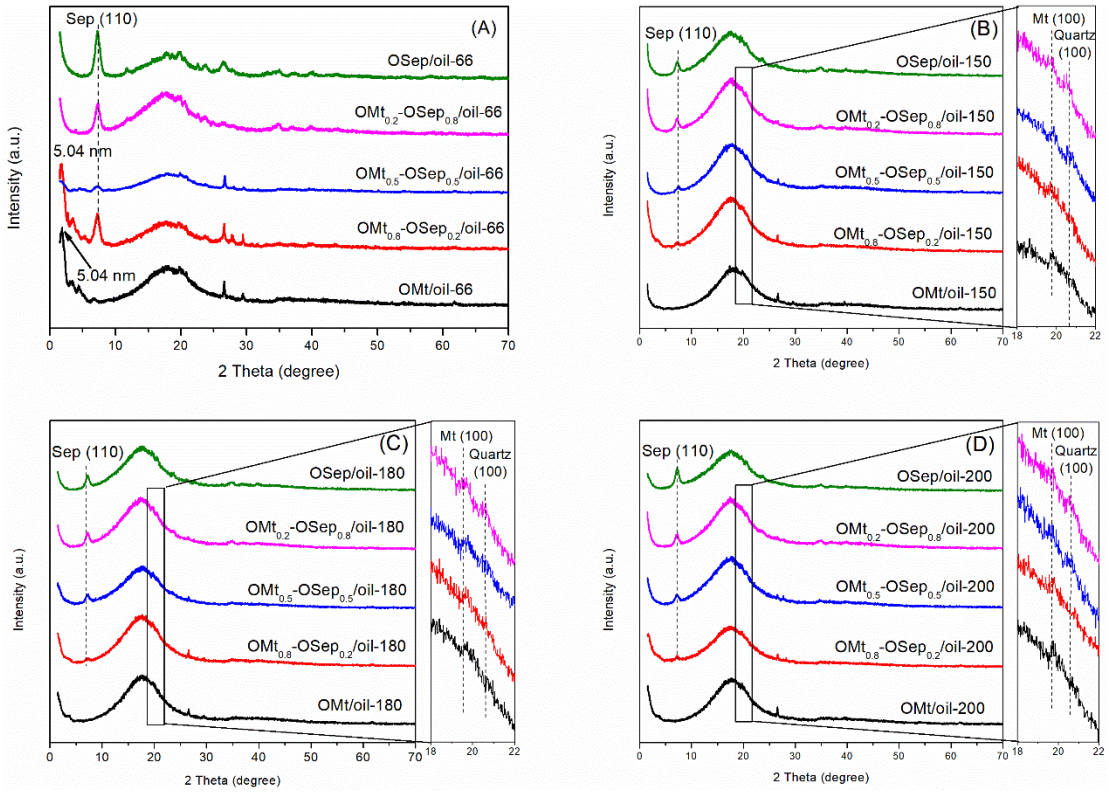

Fig. 3 XRD patterns of OC/oil gels aged at (A) 66°C, (B) 150°C, (C) 180°C and 200°C.

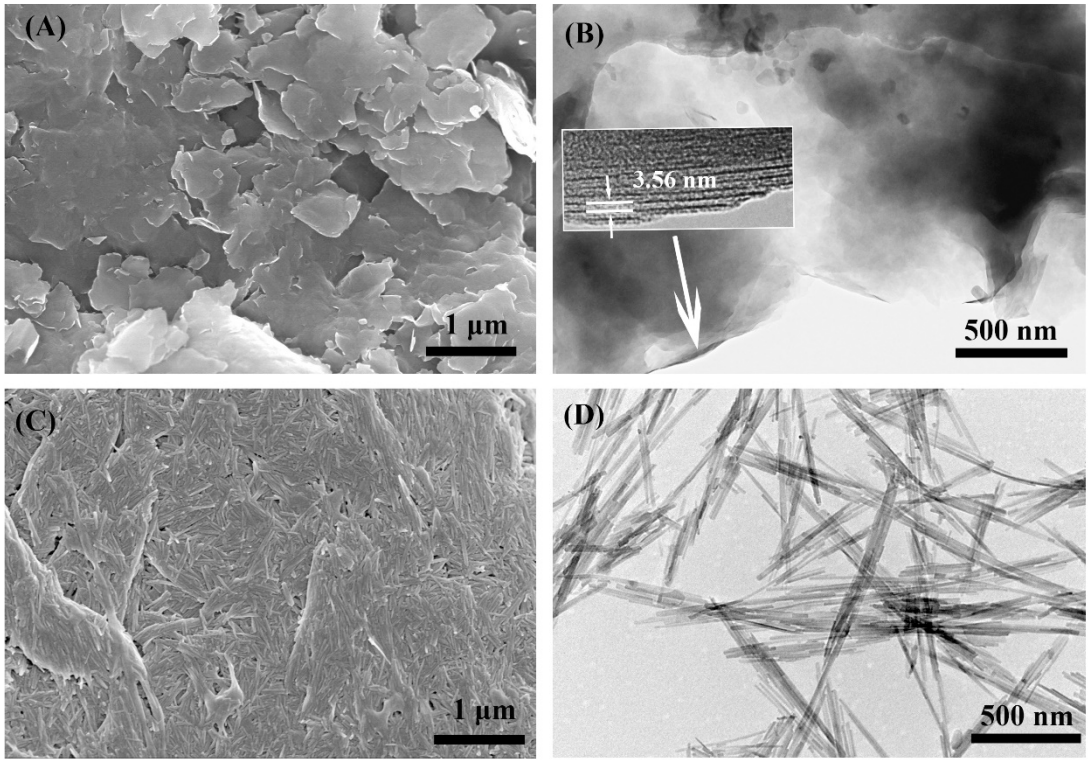

Fig. 4 SEM images of (A) OMt and (C) OSep; TEM images of (B) OMt and (D) OSep.

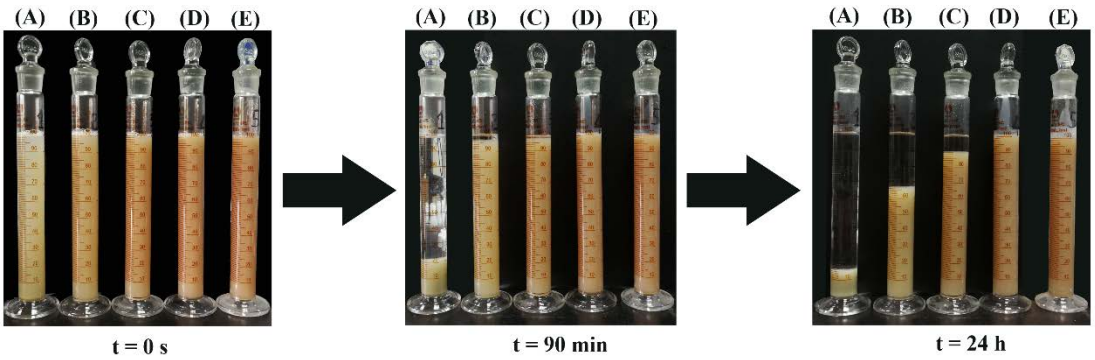

Fig. 5 Gel volume results of (A) OMt, (B) $OMt_{0.8}$-$OSep_{0.2}$, (C) $OMt_{0.5}$-$OSep_{0.5}$, (D) $OMt_{0.2}$-$OSep_{0.8}$ and (E) OSep in oil.

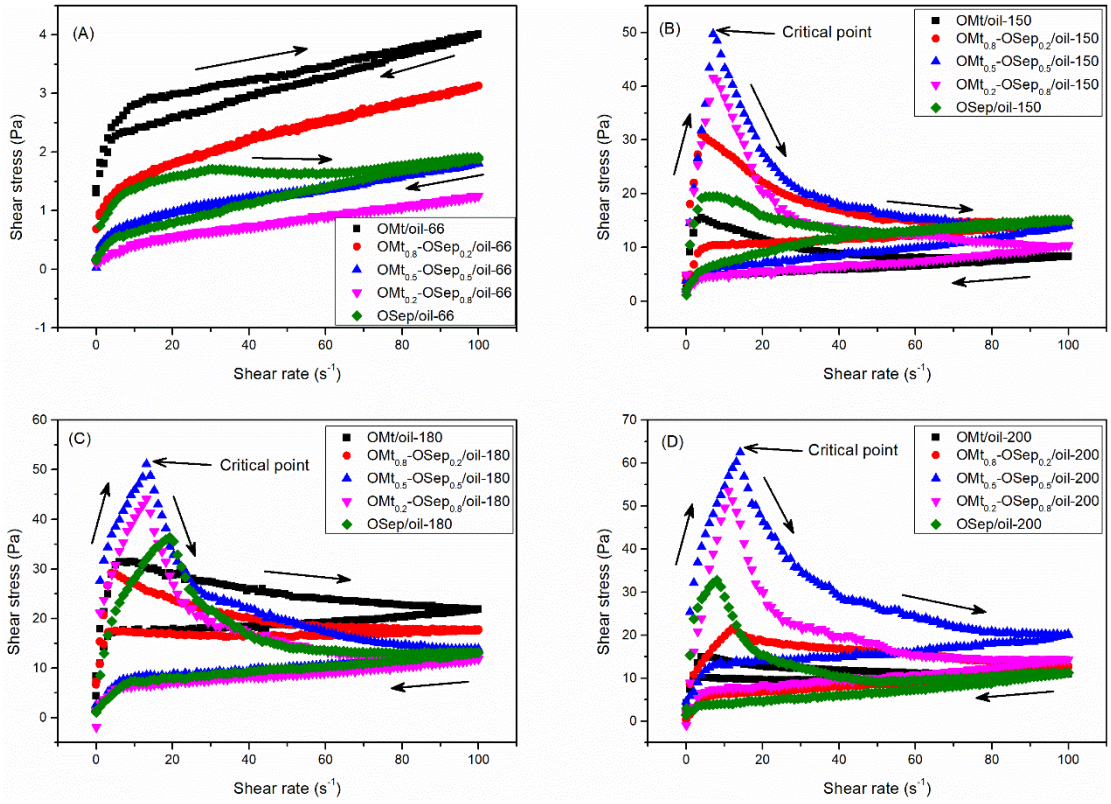

Fig. 6 Dynamic rheological curves of OC/oil fluids aged at (A) 66°C, (B) 150°C, (C) 180°C and (D) 200°C for 16 h.

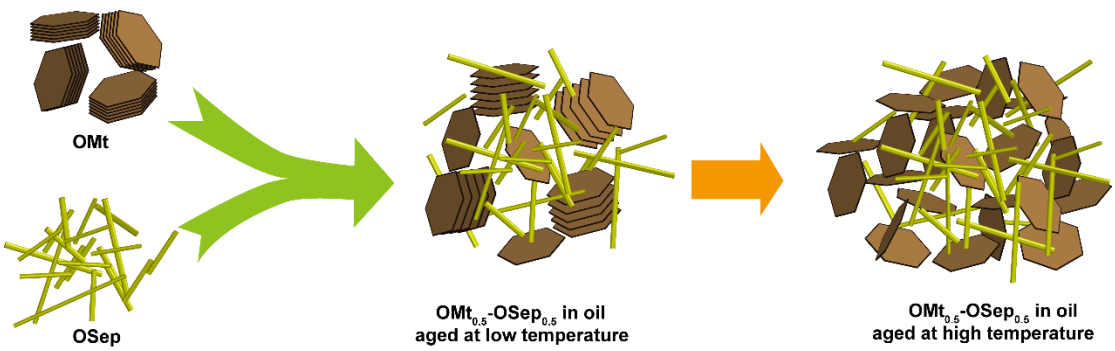

Fig. 7 the Interpretive diagram of the network structure of the mixed OMt and OSep in oil.

Figure captions:

Fig. 1 XRD patterns of (A) Mt, OMt, (B) Sep and OSep.

Fig. 2 (A) Interpretive diagram of XRD test for OC/oil gel sample and (B) XRD patterns of the sample holder and sample holder with oil.

Fig. 3 XRD patterns of OC/oil gels aged at (A) 66°C, (B) 150°C, (C) 180°C and 200°C.

Fig. 4 SEM images of (A) OMt and (C) OSep; TEM images of (B) OMt and (D) OSep.

Fig. 5 Gel volume results of (A) OMt, (B) $OMt_{0.8}$-$OSep_{0.2}$, (C) $OMt_{0.5}$-$OSep_{0.5}$, (D) $OMt_{0.2}$-$OSep_{0.8}$ and (E) OSep in oil.

Fig. 6 Dynamic rheological curves of OC/oil fluids aged at (A) 66°C, (B) 150°C, (C) 180°C and (D) 200°C for 16 h.

Fig. 7 the Interpretive diagram of the network structure of the mixed OMt and OSep in oil.

Tables

Table 1 Chemical composition of Mt and Sep (derived from XRF results)

Sample	Composition (mass %)						
	SiO_2	Al_2O_3	CaO	MgO	Na_2O	Fe_2O_3	others
Mt	64.40	19.71	4.16	3.75	3.72	3.30	0.96
Sep	63.68	9.88	1.26	19.41	0.87	3.35	1.55

Table 2 Details of the mixtures of OMt and OSep.

Sample	OMt (mass %)	OSep (mass %)
OMt	100	0
$OMt_{0.8}$-$OSep_{0.2}$	80	20
$OMt_{0.5}$-$OSep_{0.5}$	50	50
$OMt_{0.2}$-$OSep_{0.8}$	20	80
OSep	0	100

Table 3 A summary of shear stress results corresponding to the critical points.

Sample	Shear stress (Pa)			
	66°C	150°C	180°C	200°C
OMt/oil	none	15.62	31.41	15.28
$OMt_{0.8}$-$OSep_{0.2}$/oil	none	31.50	29.33	22.05
$OMt_{0.5}$-$OSep_{0.5}$/oil	none	50.12	51.08	62.67
$OMt_{0.2}$-$OSep_{0.8}$/oil	none	41.52	44.49	53.81
OSep/oil	none	19.64	36.53	33.06

Table 4 A summary of shear stress (τ) at the shear rate (γ) of 100 s^{-1}.

Sample	τ (Pa)				$\tau_{66\text{-}150}$	$\tau_{180\text{-}200}$
	66°C	150°C	180°C	200°C	(%)	(%)
OMt/oil	4.02	8.36	21.53	10.96	108	-49
$OMt_{0.8}$-$OSep_{0.2}$/oil	3.13	14.95	17.60	13.10	378	-26
$OMt_{0.5}$-$OSep_{0.5}$/oil	1.80	14.16	13.96	20.34	687	46
$OMt_{0.2}$-$OSep_{0.8}$/oil	1.25	9.95	11.78	13.86	696	18
OSep/oil	1.91	15.16	13.29	10.85	694	-18

Note: $\tau_{66\text{-}150} = (\tau_{150}\text{-}\tau_{66})/\ \tau_{66} \times 100\%$, similarly, $\tau_{180\text{-}200} = (\tau_{200}\text{-}\tau_{180})/\ \tau_{180} \times 100\%$; τ_x refers to the shear stress at 100 s^{-1} of fluids aged x°C.

Table 5 The areas of thixotropic loops (A) in Fig. 6.

Sample	A ($Pa \cdot s^{-1}$)				A_{66-150} (%)	$A_{180-200}$ (%)
	66°C	150°C	180°C	200°C		
OMt/oil	22.50	325.97	635.20	186.22	1349	-71
$OMt_{0.8}$-$OSep_{0.2}$/oil	3.46	600.86	710.46	361.12	17266	-49
$OMt_{0.5}$-$OSep_{0.5}$/oil	4.82	1097.75	1281.62	1497.10	22675	17
$OMt_{0.2}$-$OSep_{0.8}$/oil	2.39	907.37	1011.93	1080.78	37865	7
OSep/oil	39.38	275.34	842.99	644.85	599	-24

Note: $A_{66-150} = (A_{150}-A_{66})/ A_{66} \times 100\%$, similarly, $A_{180-200} = (A_{200}-A_{180})/ A_{180} \times 100\%$;

A_x refers to the area of a sample aged at x°C.